Extending the Lifetime of MEDA Biochips by Selective Sensing on Microelectrodes

Tung-Che Liang, Zhanwei Zhong, Miroslav Pajic, *Senior Member, IEEE*, Krishnendu Chakrabarty, *Fellow, IEEE*

***Abstract*—A digital microfluidic biochip (DMFB) enables miniaturization of immunoassays, point-of-care clinical diagnostics, and DNA sequencing. A recent generation of DMFBs uses a micro-electrode-dot-array (MEDA) architecture, which provides fine-grained control of droplets and real-time droplet sensing using CMOS technology. However, microelectrodes in a MEDA biochip degrade when they are charged and discharged frequently during bioassay execution. In this paper, we first make the key observation that the droplet-sensing operations contribute up to 94% of all microelectrode actuation in MEDA. Consequently, to reduce the number of droplet-sensing operations, we present a new microelectrode cell (MC) design as well as a *selective-sensing* method such that only a small fraction of microelectrodes perform droplet sensing during bioassay execution. The selection of microelectrodes that need to perform the droplet sensing is based on an analysis of experimental data. A comprehensive set of simulation results show that the total number of droplet-sensing operations is reduced to only 0.7%, which prolongs the lifespan of a MEDA biochip by 11x without any impact on bioassay time-to-response.**

I. Introduction

Digital microfluidic biochips (DMFBs) are used for biomolecular recognition, point-of-care diagnostics, and air monitoring applications [1], [2], [3]. DMFBs manipulate fluids as discrete droplets of picoliter volume using the principle of electro-wetting-on-dielectric (EWOD) [4]. Because of their precise control over microfluidic operations, DMFBs offer several key advantages, including simple instrumentation, flexible device geometry, and easy coupling with other technologies [5]. This technology has been commercialized in recent years for diagnostics and immunoassays [6], [7].

A micro-electrode-dot-array (MEDA) biochip has been proposed in recent years to further advance DMFB technology [8], [9]; an example of a fabricated chip is shown in Fig. 1. Similar to traditional DMFBs, MEDA biochips manipulate discrete fluids using EWOD. However, unlike traditional DMFBs, MEDA biochips offer fine-grained fluidic control and real-time droplet sensing [9]. The MEDA biochip consists of a large number of microelectrodes that are arranged in a regular pattern, and these microelectrodes are much smaller than the electrodes in traditional DMFBs. Multiple microelectrodes are dynamically grouped together to form a fluidic module (i.e., splitter or mixer). MEDA biochips have been fabricated using TSMC $0.35\,\mu\text{m}$ CMOS technology [9]. A 30 V power supply is used to activate microelectrodes, and 3.3 V is used as the power supply for the digital circuit that controls the microelectrodes [9].

In MEDA biochips, a real-time capacitive-sensing circuit is integrated with each microelectrode, and this is used to detect the location and size of a droplet. In every operational cycle, the sensing circuit discharges and charges the microelectrode, and measures the charging time. The charging time is used to detect whether a droplet is present over the microelectrode. To obtain the positions of on-chip droplets, the sensing results of all the microelectrodes are shifted out from a scan-chain design of the sensing circuits. In addition, the dynamic sensing capability allows high-level synthesis for real-time error recovery [10], [11], [12].

Prior work has identified a number of failure mechanisms for digital microfluidic biochips [13]. A number of these failure mechanisms are related to manufacturing defects; therefore, post-fabrication testing can be used to screen bad chips. However, defects such as microelectrode degradation can occur throughout the lifetime of the system. Because a MEDA biochip manipulates discrete fluids using the EWOD principle, microelectrodes in the biochip are continuously charged and discharged during bioassay execution. According to results presented in [14], [15], charge trapping in the dielectric layer and degradation of the insulator can result in electrode degradation during bioassay execution. Even if a biochip is immediately tested after production, electrode degradation can happen during the lifetime of the biochip. This is the most-common failure mechanism in the field and the shortest path to failure [16], [17]. If an electrode is degraded during bioassay execution, fluidic operations associated with this degraded electrode will fail, resulting in bioassay failure. To ensure reliable bioassay execution in digital microfluidic systems, prior work has focused on reducing excessive electrode charging for droplet actuation during bioassay execution [18], [19].

However, prior work does not address one of the key reasons underlying microelectrode degradation. According to the data collected for bioprotocols running on MEDA biochips, we find that droplet-sensing operations dominate the total number of charging cycles per microelectrode. Table I shows the number of microelectrode-charging cycles for three bioassays, namely multiplexed in-vitro diagnosis [20], gene-expression analysis [21], and chromatin immunoprecipitation (ChIP) [22], on a 30×60 MEDA biochip. In Table I, $A_{min}/A_{max}/A_{avg}$ is the minimum/maximum/average number of times a microelectrode is charged due to droplet actuation, and S is the number of droplet-sensing operations performed in each microelectrode. The value of $S/(S + A_{avg}) \times 100\%$ indicates proportional contribution of droplet-sensing operations

Manuscript received April 18, 2020; revised June 12, 2020; accepted July 6, 2020. This article was presented in the International Conference on Compilers, Architecture, and Synthesis for Embedded Systems 2020 and appears as part of the ESWEEK-TCAD special issue.

Tung-Che Liang, Zhanwei Zhong, Krishnendu Chakrabarty, and Miroslav Pajic are with the Department of Electrical and Computer Engineering, Duke University, Durham, NC, USA (e-mail: tung.che.liang@duke.edu; zz114@duke.edu; krish@duke.edu; miroslav.pajic@duke.edu).

This research was supported by the US National Science Foundation under grant number ECCS-1914796.

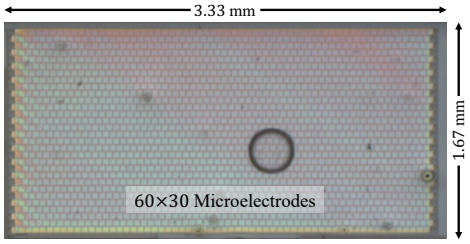

Fig. 1: Droplet on a MEDA biochip during a laboratory experiment.

to microelectrode charging. Table I shows that droplet-sensing operations contribute at least 94% of the total number of times a microelectrode is charged/discharged. Therefore, in order to prolong the lifetime of microelectrodes, it is critical to reduce the total number of droplet-sensing operations.

The work in [17] presented an analysis and experimental results on the electrode lifetime in terms of the number of electrode being charged/discharged in EWOD devices. When the dielectric layer underneath an electrode is thin, either motivated by the need to reduce the actuation voltage or due to fabrication imperfections, the electrode can only be charged up to 200 times before it is completely degraded. Complex biochemical applications, such as chromatin immunoprecipitation (ChIP), typically require hundreds of operational cycles when they are mapped to MEDA biochips. As shown in Table I, in today's MEDA biochips, a microelectrode needs to charged and discharged more than 300 times when a single bioassay is executed. As a result, a microelectrode is likely to degrade (with a failure in bioassay execution) because of the excessive charging associated with droplet actuation and droplet sensing. In fact, similar biochip degradation concerns are likely to have forced Illumina—one of the earliest adopters of DMFB technology—to halt sales of its NeoPrep platform. In a letter to customers, Illumina cited reliability issues in house and far worse ones in the field [23].

Consequently, to increase the lifetime of MEDA biochips, it is critical to eliminate unnecessary droplet-sensing operations during bioassay execution. In this paper, we show how this objective can be achieved by carrying out droplet sensing in only a small fraction of the microelectrodes, without any adverse on bioassay executions. We refer to this approach as *selective sensing*.

The key contributions of this paper are as follows:

- We develop a new microelectrode-cell (MC) design that allows us to enable/disable droplet-sensing operation for each MC on the MEDA.
- We propose a selective-sensing strategy—only a few MCs are utilized to determine droplet locations.
- We show on real-life bioassay protocols that selective sensing significantly reduces the number of times a microelectrode needs to be charged/discharged during bioassay execution. Simulation results also show that the maximum number of times a microelectrode needs to be charged/discharged is considerably reduced. As a result, the biochip lifetime is increased by 11x with no impact on bioassay time-to-results.

The remainder of this paper is organized as follows. Section II introduces the MEDA architecture. Section III presents a new MC design that allows selective sensing. Section IV describes the selective-sensing method for sensing. Section V illustrates the effectiveness of the proposed method on several commonly used complex bioassays. Section VI discusses the overhead associated with the proposed method. Finally, Section VII concludes the paper.

TABLE I: Statistics on microelectrode charging for three bioassays.

Bioassay	A_{min}	A_{max}	A_{avg}	S	$S/(S+A_{avg})\times 100\%$
Multiplexed In-Vitro Analysis	0	128	11.69	196	94%
ChIP	0	131	5.72	314	98%
Gene Expression Analysis	0	104	6.55	351	98%

II. Background

In this section, we first describe the basic unit of MEDA, i.e., the MC. Next, we explain the scan-chain architecture that connects these basic units together. We also describe how MEDA performs droplet operation using the scan-chain of microelectrode cells. Finally, we show that the droplet-sensing operation in MEDA is inefficient due to the sensing mechanism incorporated in the MC design.

A. Microelectrode Cell

The schematic of an MC is shown in Fig. 2. A typical MC includes four parts: a microelectrode, a D flip-flop (DFF), an actuation circuit, and a sensing circuit. Operations that can be performed on an MC include the following:

1) MC actuation. To perform droplet operations on MEDA, the biochip needs to activate a group of MCs to form a micro-component (e.g., splitter or mixer). In this operation, the controller sets ACT $=$ 1, IN $=$ 1, and a high voltage (e.g., 25 V) to the top plate [24]. If a rising edge of MC-CLK is applied to the DFF, pin Q is set to logic "1", and transistors T3 and T4 are switched on, while transistors T1 and T2 are switched off. In this case, the bottom plate is directly connected to ground (0 V). Because the surrounding microelectrodes are not connected to ground, the potential difference between this microelectrode and the surrounding microelectrodes generates an EWOD force that moves the droplet towards to the activated MC [25].

2) MC sensing. MC sensing is used to detect droplet locations by measuring the capacitance between the top plate and bottom plate. In this operation, the controller sets ACT $=0$, ACT_b $=1$, and SEL $=1$; the controller also connects the top plate to ground. When this happens, transistors T1, T2, and

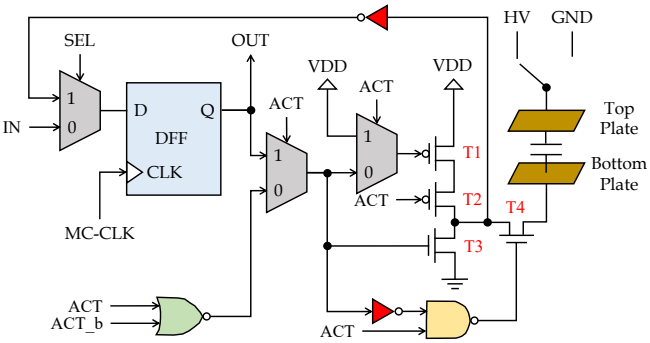

Fig. 2: Schematic of an MC in MEDA biochips.

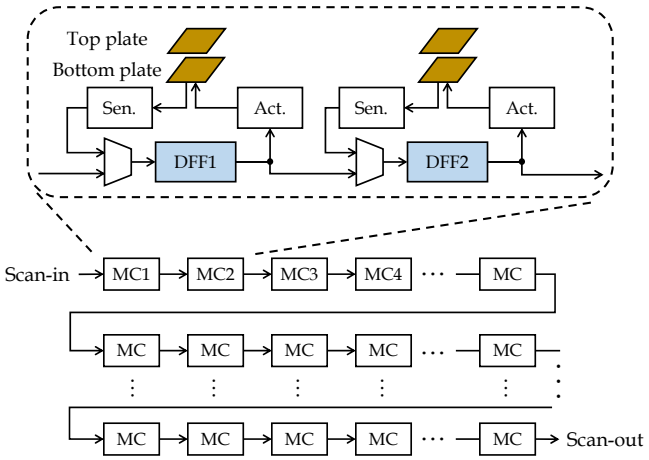

Fig. 3: An illustration of the scan-chain structure in MEDA.

T4 are switched on while transistor T3 is switched off, the bottom plate is connected to VDD (3.3 V) and the voltage of the bottom plate increases to 3.3 V. Next, the control circuit set ACT_b $= 0$, and transistors T1, T3 and T4 are switched on while transistor T2 is switched off. As a result, the bottom plate is now connected to ground, and the voltage of the bottom plate decreases due to discharging. By applying a rising edge of MC-CLK at a preset time, a value of "0" or "1" will be store in the DFF. If a droplet is present between the top plate and bottom plate, the discharge rate is slower, and a value of "1" is stored; otherwise, the DFF stores a value of "0".

The actuation status of an MC is determined by the value stored in the DFF: a value of "1" indicates MC actuation; otherwise, the MC is de-activated. In the following discussion, we refer to the actuation value for each MC as the *MC-actuation value*. After MC sensing, the result is written to the DFF indicating whether a droplet is present. In the following discussion, we refer to the capacitance measured for each MC as the *MC-sensed value*.

B. Scan-chain Design

To set the MC-actuation value to each MC and read out the MC-sensed values, all the MCs in today's MEDA platform are connected using a single scan-chain structure, i.e., the output of one MC is connected to the input of the next MC (see Fig. 3) [9]. Using this scan chain, a sequence of bits is shifted into the scan chain such that the value in each DFF can be programmed. We refer to the sequence of bits as an *actuation pattern*. Likewise, after MC-sensing operation, the 0/1 MC-sensed values are stored in each DFF. The MC-sensed values are obtained by shifting out a sequence of bits, which is referred to as a *sensed pattern*.

C. MEDA Working Principle

To carry out a bioassay (i.e., a bio-chemical experiment) on a MEDA biochip, a synthesis tool is used to generate a schedule of fluidic operations, module placement, and droplet routes for the bioassay [26]. Next, these three results are mapped to a sequence of actuation patterns. The actuation patterns are sequentially shifted to the MC array through the scan-chain structure. When the actuation pattern is applied to the microelectrodes, an induced force is created, which drags the droplet toward the activated microelectrodes based on the principle of EWOD [25]. After an actuation pattern is activated on the MC array, all the MCs are set to the sensing mode. The sensing results of all the MCs are scanned out as feedback to validate the effectiveness of the fluidic operation [9], [27]. The process of shifting an actuation pattern, activating MCs, droplet sensing, and shifting the sensing results is referred to as an *operational cycle*, and the operational cycle is repeated until the completion of the bioassay.

D. Motivation: Increasing MEDA Lifetime

Microelectrode degradation is inevitable if microelectrodes are excessively actuated during bioassay execution [18], [19]. Therefore, previous work has focused on reducing excessive electrode charging for droplet actuation. The work in [18] presented a module-placement method that can prevent excessive use of certain electrodes. Recently, the work in [19] presented a block-aware synthesis method based on IEEE Std. 1687 network design. This method first divides the microelectrodes into several blocks and then uniformly utilizes these blocks throughout bioassay execution. Although the experimental results in Table I show that droplet-sensing operations are the predominant contributor to microelectrode degradation, these methods, however, neglect the microelectrode charging associated with droplet sensing.

For today's MEDA biochips, we can manipulate fluids in a fine-grained manner because we can control the actuation status of each MC individually by writing an MC-actuation value to each DFF [28], [29]. However, during droplet sensing, all the MCs must simultaneously carry out the sensing operation. It is often the case that, during the execution of a bioassay, droplets occupy only a small fraction of MCs in the array. If all MCs are used to sense the location of droplets in each step of bioassay execution, the lifetime of a MEDA biochip will be significantly reduced because frequent charging of an MC induces charge trapping and microelectrode degradation [17].

For example, in Fig. 1, all the 1800 MCs are charged and discharged in the droplet-sensing operation every clock cycle. However, as can be seen in the figure, the droplet occupies only 40 MCs, and if we perform droplet sensing only on the corresponding MCs, we can reduce the number of MCs that are used for droplet sensing by 97%. In the next section, we introduce a new MC design such that we are able to selectively turn on/off the MC-sensing function for each MC.

III. MC Design for Selective Sensing

In this section, we propose a new MC design such that we can enable/disable the droplet-sensing operation for each MC, i.e., the new MC can support selective sensing for MEDA.

A. New MC Design

Recall that by controlling the DFF in Fig. 2, we can enable/disable the MC for droplet actuation. The schematic of the new MC is shown in Fig. 4. Compared with the original MC design shown in Fig. 2, we add a three-input OR gate and a control signal $F2G$ (i.e., Force-to-Ground) to the MC circuit. This signal is used to force the microelectrode voltage to ground after the sensing operation is completed.

Supposed an MC is in the sensing mode, where the control

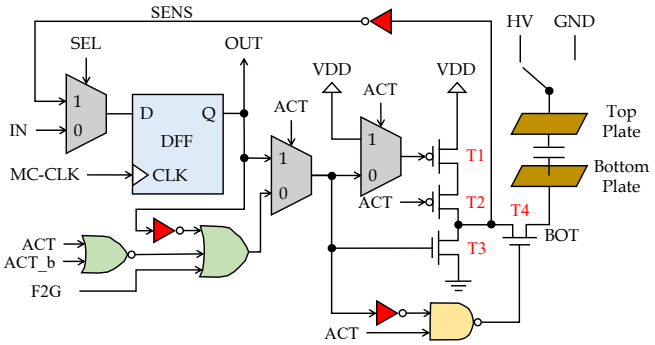

Fig. 4: New microelectrode-cell design for selective sensing.

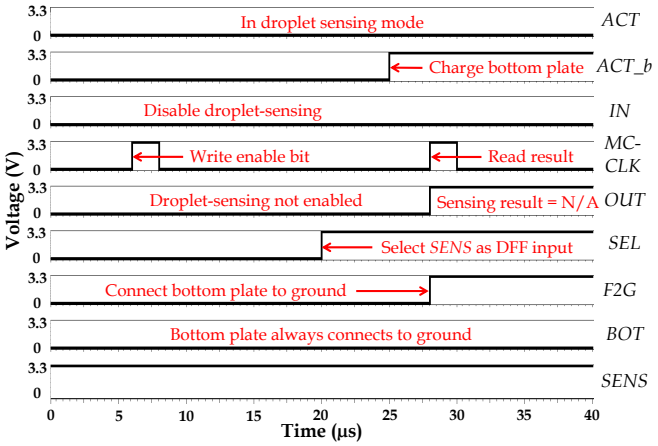

Fig. 5: Simulation results when droplet-sensing operation is disabled.

signal ACT changes from 1 to 0, and the control signal $F2G = 0$. Therefore, transistors T2 and T4 are switched on. To measure the capacitance of the microelectrode, we need to first charge the microelectrode and then discharge the microelectrode, i.e., T1 needs to be switched on and then T3 needs to be switched on. The value stored in DFF determines the output of the three-input OR gate and thus whether T1 will be switched on. When the DFF stores "0", T1 will be switched off, and T3 will be switched on. Therefore, microelectrode charging for sensing can be avoided.

On the other hand, when the DFF stores "1", the output of the three-input OR gate is determined by the output of the logical NOR of ACT and ACT_b, which is the same as in the conventional MC design. Therefore, the sensing operation can now be carried out. After the sensing operation is completed, the $MC - CLK$ signal is fed to the MC such that "1" is stored in the DFF when a droplet is present; otherwise, "0" is stored in the DFF. Finally, $F2G$ is set to 1 to ensure that T3 is on and the microelectrode is not charged because of the new value stored in the DFF.

B. Design Validation using HSPICE Simulation

We evaluated the MC design of Fig. 4 using HSPICE and a 350 nm library from a foundry that matches the fabricated prototypes. The simulation results (see Fig. 5 and Fig. 6) as well as the new working principle are described as follows.

1) Droplet-sensing disabled. In this operation (illustrated in Fig. 5), a "0" value is first shifted in to the MC using the scan-chain, and the '0' value of OUT indicates that droplet-sensing operation is disabled. Therefore, for the sensing-

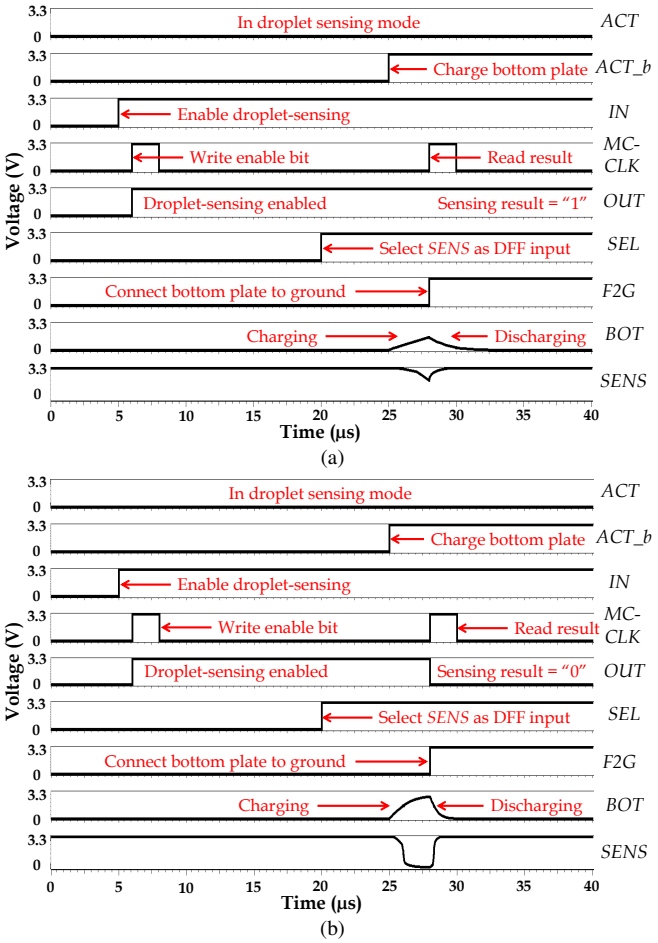

Fig. 6: Simulation results for the droplet-sensing operation: (a) with a droplet, and (b) without a droplet.

mode period, the bottom plate is always connected to ground. Because of the global signal $F2G$, the bottom plate is always connected to ground even though the value of OUT changes for the second rising edge of $MC - CLK$.

2) Droplet-sensing enabled (with a droplet). In this operation (illustrated in Fig. 6(a)), a "1" value is first shifted in to the MC using the scan-chain, and the '1' value of OUT indicates that droplet-sensing operation is enabled. As a result, when $ACT\_b = 1$, the bottom plate is connected to VDD (3.3 V), and the voltage of net BOT is rising because of capacitor charging. Note that the presence of a droplet increases the dielectric constant, and the capacitor requires longer time to charge. When a second rising edge of $MC - CLK$ is applied, the sensing output $SENS$ is still in a high voltage level. Therefore, an MC-sensed value of "1" is store in the DFF, which indicates that a droplet is present.

3) Droplet-sensing enabled (without a droplet). In this operation (illustrated in Fig. 6(b)), a "1" value is first shifted in to the MC using the scan-chain, and the "1" value of OUT indicates that droplet-sensing operation is enabled. As a result, when $ACT\_b = 1$, the bottom plate is connected to VDD (3.3 V), and the voltage of net BOT is rising because of capacitor charging. Without a droplet present, the dielectric constant is smaller and it takes less time to charge the capacitor. When a second rising edge of $MC - CLK$ is applied, the sensing

output $SENS$ is at a low voltage level. Therefore, an MC-sensed value of "0" is store in the DFF, which indicates that no droplet is present.

IV. Selective Droplet Sensing

The new MC described in Section III enables MEDA to perform selective sensing during bioassay execution. We next present a selective-sensing method that can reduce the use of MCs for sensing. Because droplets are dynamically moved on the MEDA biochip during bioassay execution, our selective-sensing method first dynamically chooses MCs that are associated with the fluidic operations. Our method selects these MCs at each operational cycle according to the pre-determined synthesis results, i.e., actuation patterns. Assuming that T operational cycles are required for bioassay execution, we define the t^{th} operational cycle as the time step t, where $1 \leq t \leq T$. A time step therefore refers to a clock cycle.

A. Determining Sensing Regions During Bioassay Execution

As discussed in Section II, the time required to execute each fluidic operation of a bioassay is determined by the synthesis tool before bioassay execution. We analyze all the fluidic operations, namely droplet dispensing, droplet discarding, droplet transportation, droplet merging, and droplet splitting, cycle by cycle and identify which microelectrodes need to be used in each time step.

Introducing/Discarding Droplets to/from MEDA

1) Droplet-dispensing operation. Droplets are introduced to the MEDA biochip by *dispensing modules* [30], [31]. Note that the locations of dispensing modules are pre-determined and droplet-dispensing operations are accurate [31] (e.g., it has been demonstrated experimentally that volumetric variations are negligible). Therefore, the MCs that are used for droplet dispensing are always fixed. We define the set of MCs used for a droplet-dispensing operation at time t as DD_t.

2) Discarding-a-droplet operation. Similar to the dispensing operation, waste fluids are generated during bioassay execution. These droplets are collected in a waste reservoir. Therefore, the MCs used for discarding a droplet are always fixed. We define the set of MCs that are used for a discarding-a-droplet operation at time t as DI_t.

Droplet Manipulation on MEDA

After a droplet is dispensed, the location of the droplet can be monitored using sensing operations. Therefore, for the operations described below, we assume that the location of a droplet has been identified using the sensing results obtained at the previous time step. The set of the MCs over which droplets are present at time t is denoted as DL_t.

3) Droplet-transportation operation. An example is shown in Fig. 7(a), in which an actuation pattern is applied to move a droplet to the right. In most cases, the droplet can be successfully moved to the desired location. However, it has been shown that due to subtle variations and imperfections in biochips [16], the induced EWOD-force may not be strong enough to move the droplet to the desired location. In this case, the droplet is 'stuck' at the original location.

The red bounding box in Fig. 7(a) shows the location range for the droplet after the actuation pattern is applied. We conclude that to obtain the droplet location after we apply an actuation pattern, we need to sense only the MCs that appear within the bounding box.

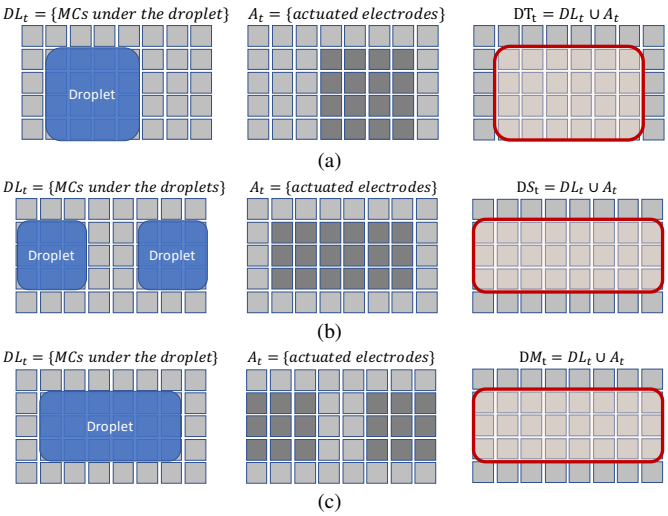

Fig. 7: Sensing regions (in red rectangles) for (a) droplet transportation, (b) droplet merging, and (c) droplet splitting.

TABLE II: Comparison between all the fluidic operations.

Operation Type	Set of MCs for selective sensing
Dispensing	DD_t
Discarding-a-droplet	DI_t
Transportation	$DT_t = DL_t \cup A_t$
Merging	$DM_t = DL_t \cup A_t$
Splitting	$DS_t = DL_t \cup A_t$

We define the set of MCs that are used by the actuation pattern at time t as A_t. We define the set of MCs that are used for transportation operations at time t as DT_t. It can be easily seen that $DT_t = DL_t \cup A_t$.

4) Droplet-merging operation. An example of this operation is shown in Fig. 7(b), in which an actuation pattern is applied to merge two droplets. Similar to droplet transportation, this operation may fail due to on-chip variations and imperfections [16]. The red bounding box in Fig. 7(b) shows the location range for the droplet after we apply the actuation pattern. We conclude that, to obtain the droplet location after we apply an actuation pattern, we need to sense only the MCs that appear within the bounding box. We define the set of MCs that are used for droplet-merging operations at time t as DM_t. It can be easily seen that $DM_t = DL_t \cup A_t$.

5) Droplet-splitting operation. An example of this operation is shown in Fig. 7(c), in which an actuation pattern is applied to split a droplet into two halves. Similar to droplet transportation and droplet merging, this operation may fail due to biochip imperfections [12]. The red bounding box in Fig. 7(c) shows the location range, i.e., the set of MCs over which the resultant droplets might reside. Therefore, to obtain the droplet location after we apply an actuation pattern, we need to sense only the MCs that appear in the bounding box. We define the set of MCs that are used for droplet-splitting operations at time t as DS_t, where $DS_t = DL_t \cup A_t$.

The comparison between all the fluidic operations is presented in Table II. By analyzing all the fluidic operations and the associated sensing regions, we define the set of MCs that

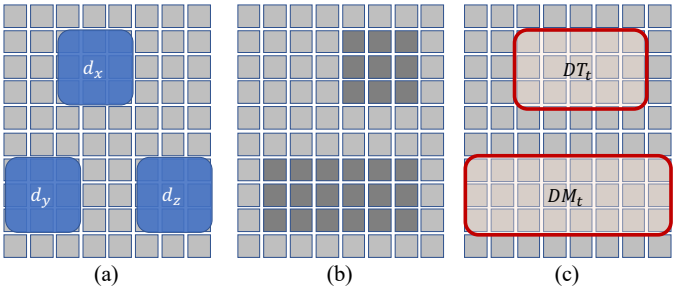

Fig. 8: An example to show that the proposed method selects a fraction of all MCs for a droplet-transportation operation and a droplet-merging operation at time t. (a) Three droplets, namely d_x, d_y, and d_z are present on the MC array. (b) The corresponding actuation patterns for the two fluidic operations. (c) The MCs that are selected for sensing are bounded by the two red rectangles.

need to be sensed at time step t as SR_t, where

$$SR_t = DD_t \cup DI_t \cup DT_t \cup DM_t \cup DS_t. \quad (1)$$

Example: Fig. 8 shows that a droplet-transportation operation and a droplet-merging operation are carried out at time t. A droplet d_x is being moved to the right, and two droplets, d_y and d_z, are being merged. Fig. 8(a) shows their positions, and Fig. 8(b) shows the corresponding actuation patterns for the two fluidic operations. According to Operation (3) and Operation (4), the associated sensing sets, DT_t and DM_t, can be derived; see Fig. 8(c). Note that because only these two types of operations are carried out at time t, $DD_t = \emptyset$, $DI_t = \emptyset$, and $DS_t = \emptyset$. Therefore, the set of MCs that are used for sensing at time t can be derived as $SR_t = DT_t \cup DM_t$.

B. Selective Sensing using Diagonal Groups

In the first step of our selective-sensing method, we utilize only a fraction of all the MCs during bioassay execution, i.e, using the MCs in SR_t. In the second step, our method can further reduce the usage of the MCs in SR_t. Intuitively, the key idea is that we do not need to select all the MCs within SR_t to acquire the droplet location. However, the selected MCs in this step need to provide the same information about the droplet location that we would get by sensing all the MCs.

Consider an example in Fig. 9, where a droplet is present on a MEDA biochip. Note that we consider an ideal situation where droplets have square shapes, but this is only for the sake of illustration. We show in Section V-A that the proposed method can be used for realistic experiments on MEDA biochips. In Fig. 9(b), 25% of the MCs are selected for sensing. However, two possible droplet locations can provide the same sensing results. As a result, this selection of MCs cannot inform us the actual droplet location. In Fig. 9(c), a different set of MCs (but still 25% of the total number of MCs) is selected for sensing. In this case, we are able to locate the droplet accurately using the sensing results. Therefore, it is important to select the MCs that provide the most information for selective sensing.

To prolong the biochip lifetime, it is critical to distribute the sensing operations evenly among the different MCs in the array. If MCs are not carefully chosen for selective sensing, as discussed in Section II-D, it is possible that some MCs will be actuated more frequently, leading to rapid microelectrode

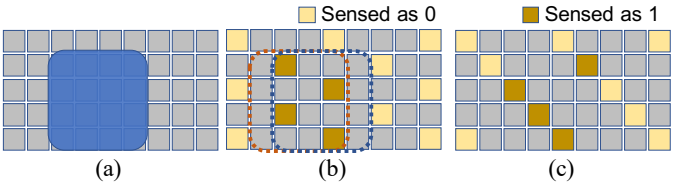

Fig. 9: Two selections of 25% of the MCs in an array for droplet sensing. The selected MCs are colored yellow and brown. (a) A droplet is present on a MEDA biochip. (b) A selection of MCs that cannot precisely identify the actual droplet location. The sensing results show that there are two possible droplet locations. (c) A selection of MCs that identifies the exact droplet location.

degradation and lifetime reduction. In the second step of our selective-sensing method, our two goals are: 1) select MCs that provide the most information, and 2) evenly distribute the sensing operations to the MCs. We achieve these two goals by selecting MCs in a specific diagonal pattern.

Consider an $N \times M$ array of MCs, where the MC at row i and column j is denoted as $mc_{i,j}$, $1 \leq i \leq N$, and $1 \leq j \leq M$. Here, we define a *diagonal line* $\mathbb{DL}(C)$ as a set of MCs such that the difference between the row and column indices is a constant integer C, i.e., $\mathbb{DL}(C) = \{mc_{i,j} \mid i - j = C\}$. For an $N \times M$ biochip, there are $N + M - 1$ diagonal lines: $\mathbb{DL}(-M+1)$, $\mathbb{DL}(-M+2)$, ..., and $\mathbb{DL}(N-1)$.

Next, these $N + M - 1$ diagonal lines are assigned to a given number (N_G) of groups, and the indices of these groups are from 1 to N_G. The k^{th} group is $G_k = \{\mathbb{DL}(C) \mid (C \mod N_G) + 1 = k\}$. An example of MC-grouping is shown in Fig. 10, where $N = 5$, $M = 10$. The array consists of a total of 14 diagonal lines. If we are given $N_G = 4$, we divide these diagonal lines into four groups. Consider two cells: $mc_{1,1}$ and $mc_{2,1}$. According to the above group-assignment rule, $mc_{1,1}$ is assigned to G_1 because it is in $\mathbb{DL}(0)$ and $(0 \mod 4)+1 = 1$. Similarly, $mc_{2,1}$ is assigned to G_2 because it is in $\mathbb{DL}(1)$ and $(1 \mod 4) + 1 = 2$. Since each group forms a diagonal spatial pattern, we refer to it as a *diagonal group*.

Next, we show how to use the diagonal groups to precisely detect the locations of droplets. Because MEDA biochips (including the sensing circuits) are thoroughly tested before bioassay execution, e.g., using the structural test method presented in [32], we assume that the sensing results of an MC are accurate. The MC returns "1" if a droplet is present; otherwise, it returns "0". While droplets can evaporate over

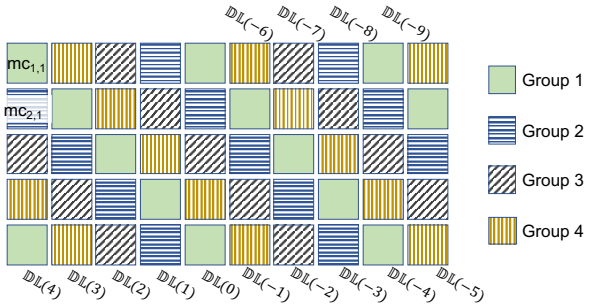

Fig. 10: An illustration of 14 diagonal lines in a 5×10 MEDA. The 14 diagonal lines are partitioned into four diagonal groups.

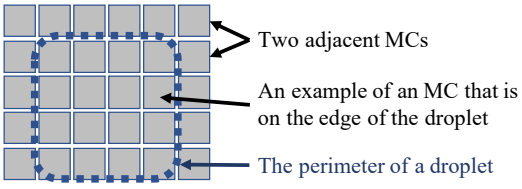

Fig. 11: Illustration of the terminology used in the lemmas.

time [33], silicone oil is used in MEDA biochips as a filler medium to prevent droplet evaporation [9]. Note that it takes less than five minutes for complex bio-protocols, such as multiplex in-vitro analysis, to be executed on MEDA biochips. The work in [33] showed that the diameter of a droplet is reduced by less than 1.2% after five minutes if silicone oil is used, i.e., droplet evaporation on MEDA biochips is negligible. Therefore, we assume that after a droplet is generated (either by dispensing, splitting, or merging), the droplet volume does not change until it is merged, split, or discarded from the MEDA biochip. Because the gap between the top plate and the MEDA array is fixed, the footprint (area) of a droplet over the MC array is also constant. Finally, due to the EWOD actuation mechanism, we assume that the droplet is in the shape of rectangles on the MC array.

We lead up to our key theorem by providing two lemmas. These lemmas reveal the relationships between the diagonal groups and droplets. We first introduce some notation used in the lemmas. Let n_d and m_d be the width and the length, respectively, of the rectangular footprint of droplet d. On the MEDA platform, the work in [12] showed that there is a minimum-sized droplet that can be dispensed and manipulated. We define the smallest droplet that can be manipulated to be of size $n_{min} \times n_{min}$. The quantity n_{min} has been experimentally demonstrated to be 2 for a specific generation of MEDA biochips [12]. For other MEDA biochips, it can likewise be determined through experimental calibration. We define $mc_{i,j}$ to be adjacent to $mc_{x,y}$ if and only if $|i-x|+|j-y|=1$. We also define $mc_{i,j}$ to be on the edge of a droplet d if $mc_{i,j}$ is under d but one of its adjacent MCs is not under d. An illustrative example of the above notation is shown in Fig. 11.

Lemma 1. *A droplet d of size $n_d \times m_d$ can be present over at most $n_d + m_d - 1$ diagonal groups.*

Proof: The proof is straightforward because we can count the MCs that are on one of the vertical edges and one of the horizontal edges of droplet d. There are n_d MCs that are located on the vertical edge. Similarly, m_d MCs are located on the horizontal edge. Note that one MC is double counted at the corner of the two edges. Therefore, a droplet can be present over at most $n_d + m_d - 1$ diagonal groups. ■

Lemma 2. *A diagonal group can precisely locate the droplet if and only if MCs in the diagonal group are located on the four edges of the droplet.*

Proof: ($\Rightarrow$) We present a proof by contradiction. Consider the two cases when MCs of a diagonal group are not located on the four edges of the droplet. 1) The droplet is not present over any MC of the diagonal group. In this case, the sensing result does not reveal the droplet location. 2) The MCs in the diagonal group can only be located on the two edges of the droplet. In this case, there are two possible locations for the droplet. The droplet can be present over one of the two sides of the diagonal group. As a result, we cannot unambiguously identify the droplet location.

($\Leftarrow$) The proof is straightforward. If microelectrodes in a diagonal group pinpoint the four edges of a droplet, we can easily infer the droplet location. ■

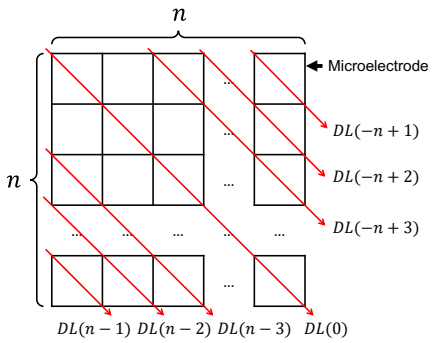

Fig. 12: Illustration of an $n \times n$ droplet with diagonal lines.

According to Lemma 1, an $n \times n$ droplet is present over a total of $2n-1$ diagonal lines. As shown in Fig. 12, we denote the diagonal lines as $\mathbb{DL}(-n+1)$, $\mathbb{DL}(-n+2)$, ..., $\mathbb{DL}(n-1)$, respectively. The quantity N_G actually determines the distance between two neighboring diagonal lines in the same group, e.g., $\mathbb{DL}(0)$, $\mathbb{DL}(N_G)$ and $\mathbb{DL}(-N_G)$ are in the same diagonal group. According to Lemma 2, in order to precisely detect the location of a droplet, MCs in a diagonal group need to be on the four edges of the droplet, i.e., the diagonal lines in a diagonal group need to "go across" the four edges of the droplet. For a small value of N_G, the interval between diagonal lines corresponding to the same diagonal group is small, and there are multiple diagonal lines in a diagonal group that "go across" the four edges. However, when the value of N_G increases, the number of diagonal lines in a diagonal group that "go across" the edges decreases. The goal here is to find the **maximum** value of N_G (i.e., the interval of diagonal lines) such that diagonal lines in a diagonal group "go across" the edges of the droplet.

Theorem 1. *Consider an $N \times M$ MEDA biochip in which there are $N + M - 1$ diagonal lines of MCs. Suppose we assign these diagonal lines of MCs into N_G **diagonal groups**, and the minimum droplet size is $n_{min} \times n_{min}$. Then we can precisely locate any droplet on a MEDA biochip if $1 \leq N_G \leq n_{min}$.*

Proof: Assume that $\mathbb{DL}(n-1)$ is used to locate a droplet of size $n \times n$. The next neighboring diagonal line (in the same diagonal group) needs to be any one of $\mathbb{DL}(n-2)$, $\mathbb{DL}(n-3)$, ..., and $\mathbb{DL}(-n+1)$. As a result, the set of available values for N_G can be expressed as $\mathbb{S}(n-1) = \{i \mid 1 \leq i \leq 2n-2\}$. Similarly, to locate the droplet using $\mathbb{DL}(n-2)$, the next neighboring diagonal line needs to be any one of $\mathbb{DL}(n-3)$, ..., and $\mathbb{DL}(-n+1)$. Therefore, $\mathbb{S}(n-2) = \{i \mid 1 \leq i \leq 2n-3\}$. The set of available values for N_G corresponding to a diagonal line $\mathbb{DL}(C)$ is: $\mathbb{S}(C) = \{i \mid 1 \leq i \leq C+n-1\}$. In order to precisely detect the droplet of size $n \times n$, the set of values for

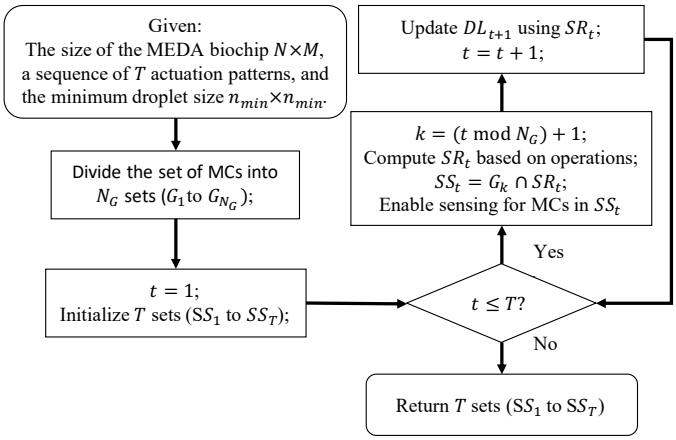

Fig. 13: The overall flow for the selective-sensing method.

N_G can be expressed as:

$$\begin{aligned} \mathbb{S} &= \mathbb{S}(n-1) \cap \mathbb{S}(n-2) \cap \ldots \cap \mathbb{S}(1) \\ &= \mathbb{S}(1) = \{i \mid 1 \leq i \leq n\} \end{aligned} \tag{2}$$

As a result, for an $n \times n$ droplet, if $N_G \in \mathbb{S}$, we are able to precisely detect the droplet location; the maximum value for N_G is n. To locate all sizes of droplets, we need to be able to locate the minimum-sized droplet ($n_{min} \times n_{min}$). Therefore, $1 \leq N_G \leq n_{min}$. ■

C. Steps Associated with Selective Sensing

We assume that we are provided with the following information: 1) the size of the MEDA $N \times M$; 2) a sequence of actuation patterns (A_1 to A_T) for a specific bioassay, generated by a synthesis tool; 3) the minimum size $n_{min} \times n_{min}$ of a droplet that can be used in bioassay execution. Our method consists of two steps:

Step 1: The selective-sensing method first generates sensing regions where droplets may be located in each operational cycle as described in Section IV-A. Therefore, we can obtain SR_t using Equation (1), where $1 \leq t \leq T$.

Step 2: We partition the $N \times M$ MCs into N_G groups, where $N_G = n_{min}$, as described in Section IV-B. Recall that the set of MCs that are assigned to the k^{th} group is referred to as G_k. Assume that the bioassay requires a total of T actuation patterns. At time t, only the MCs in G_k are used for sensing, where $1 \leq t \leq T$ and $k = (t \bmod N_G) + 1$. Therefore, the set of MCs that need to perform droplet sensing at time t is denoted by SS_t, where $SS_t = SR_t \cap G_k$. The overall flow for selective sensing is shown in Fig. 13.

V. Experimental Results

We first validate the proposed selective-sensing method using experimental data obtained from fabricated MEDA biochips. We then evaluate the effectiveness of the proposed method using three real-life biochemical protocols.

A. Validation Using Experimental Data

As described in Section III, when a droplet is being sensed, there is no EWOD force applied to the droplet. Therefore, the shape of a droplet is nearly a sphere because of the cohesive forces originated from the surface layer [34]. While some microelectrodes are fully covered by the droplet, some microelectrodes are partially covered by the droplet. The

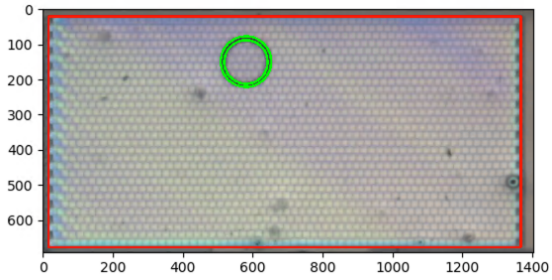

Fig. 14: Droplet location is computed using an image-processing tool. The droplet is identified and highlighted in green. The biochip array is identified and highlighted in red.

EWOD technology requires such partial overlap to enable droplet movement. In Section IV-B, we assume that the droplet has a rectangular shape as a simplification because we are only interested in the x-y directions and we are not studying any forces in the vertical dimension. The microelectrodes within the rectangle area are fully covered by the droplet. The simplified rectangular shape is a conservative choice from the localization perspective and justified by the fact that we are only modeling forces that move droplets in the x- and y- directions. No diagonal forces or diagonal movements are being considered. Theorem 1 shows that we can precisely locate a droplet (in the form of a rectangle) using selective sensing with a few diagonal groups. Because the actual droplet footprint (a circle) is larger than the rectangle, we can also precisely locate the droplet using the same number of diagonal groups. In this subsection, we show that fluidic-operation snapshots obtained from fabricated MEDA biochips corroborate this assessment.

We executed fluidic operations on a fabricated MEDA biochip with droplets whose diameter is n microelectrodes ($6 \leq n \leq 14$). The videos of droplet operations were captured by a CCD camera, and we analyzed the videos using image-processing techniques. The software package OpenCV [35] was used to identify droplet locations. The droplet location is defined as a set of microelectrodes that are completely covered by the droplet. An example of droplet localization is shown in Fig. 14. A total of 410 fluidic operations were captured, and the droplet locations and the associated actuation patterns were stored as the data set.

We next propose a metric to evaluate whether a diagonal group (G_k) can accurately locate the droplet positions for all the fluidic operations in the data set. A fluidic operation in the data set contains three parts: 1) the droplet location before actuation, 2) the actuation pattern, and 3) the droplet location after actuation. We derive the sensing regions corresponding to a fluidic operation (SR_t) based on the droplet location before actuation and the actuation pattern (as described in Section IV-A). Using the selective-sensing method, we can obtain the MCs used for sensing. Recall that the set of MCs that are used for sensing is defined as $SS_t = G_k \cap SR_t$. Using SS_t, we can obtain the sensing result corresponding to the actual droplet location after actuation. The resulting droplet location (set of microelectrodes) is referred to as R_{golden}. We then enumerate all the other possible droplet locations and use SS_t to see if the sensing result is the same as R_{golden}. The sensing result of a possible droplet location (also set of microelectrodes) is referred to as R_p. Let c be the number of cases for which

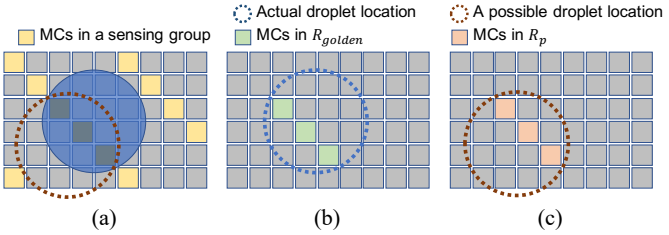

Fig. 15: Illustration of the notation used in diagonal-group evaluation. (a) A droplet is present on a MEDA biochip. The sensing result suggests that there are two possible droplet locations. (b) The actual droplet location with the corresponding R_{golden}. (c) Another possible droplet location with the corresponding R_p.

$R_p = R_{golden}$. If G_k provides the precise location of a droplet, $c = 1$; otherwise, $c > 1$. The metric $acc = 1/c$ is defined to evaluate whether G_k can accurately locate droplet positions. Consider the example shown in Fig. 15, where two possible droplet locations can result in the same sensing result. Therefore, $c = 2$, and $acc = 1/2$.

We evaluated the proposed method by varying the selective percentage p over the 410 fluidic operations in the data set, where $p = f_n/f_d$. The denominator f_d is the total number of diagonal groups (see Section IV-B), and the numerator f_n is the number of diagonal groups that we use for droplet sensing. For a given percentage p, we enumerated all the $\binom{f_d}{f_n}$ combinations, ran all these combinations on the 410 fluidic operations, and obtain the average acc for a total of $\binom{f_d}{f_n} \times 410$ experiments. The results as well as the variance bars are shown in Fig. 16. Our results show that when $p \geq \frac{1}{4}$, $acc = 1.0$. Therefore, we can obtain precise droplet locations using only 25% of the MCs, i.e., we can choose $N_G = 4$ for realistic fluidic operations.

B. Evaluation on Bioassay Protocols

We simulated the execution of three real-life biochemical protocols on a 30×60 MEDA biochip: multiplexed in-vitro diagnosis [20], gene-expression analysis [21], and chromatin immunoprecipitation (ChIP) [22]. During bioassay execution, we employed the proposed selective-sensing method and recorded the number of times each microelectrode is sensed. For the bioassay execution, we consider droplets of typical size with a diameter of six microelectrodes. We implemented the simulator using Python on a workstation with a 2.5 GHz Xeon processor and 2 GB memory.

As recent work in [19] has shown that the number of sensing operations can be reduced during bioassay execution,

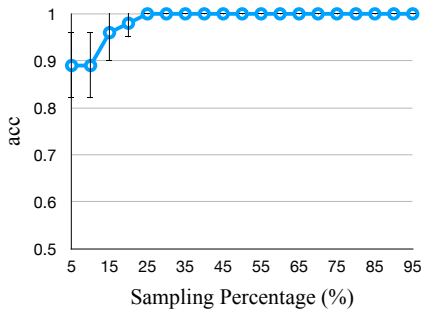

Fig. 16: Evaluation of selective sensing.

TABLE III: The number of sensing operations during bioassay execution. Comparison between the baseline method, [19], and selective sensing.

Methods	Baseline			[19]			Proposed Method		
Bioassay	Min.	Avg.	Max.	Min.	Avg.	Max.	Min.	Avg.	Max.
Multiplexed In-Vitro	196	196	196	41	144.39	196	0	2.87	26
ChIP	314	314	314	64	132.67	226	0	1.45	28
Gene Expression	351	351	351	75	125.22	194	0	1.69	21

we show the effectiveness of our method by comparing our results with [19] as well as a baseline that senses all the microelectrodes in every cycle. In this section, we first show that the number of sensing operations can be considerably reduced using the selective-sensing method. Next, we show that the lifetime of MEDA biochips can be sustantially extended using selective sensing.

1) Number of Sensing Operations Per Microelectrode

The results obtained for the number of sensing operations per microelectrode are shown in Table III. In the baseline sensing approach, each microelectrode needs to be sensed more than 100 times during bioassay execution. Although the work in [19] can reduce the number of sensing by dynamically enabling a few of the sub-daisychains in MEDA during bioassay execution, each microelectrode still needs to be sensed more than 100 times during bioassay execution. However, using the proposed method, each microelectrode only needs to be sensed less than three times on average. The number of sensing operations per microelectrode for selective sensing is only 0.7% of that for the baseline.

Fig. 17 shows the number of sensing operations for each microelectrode for different bioassays; we compare the proposed method with [19]. Fig. 17(a) shows that when [19] is used, some microelectrodes can still be charged nearly 200 times. On the other hand, using selective sensing, the number of charging operations is 6x less for all the microelectrodes. It is noticeable that many microelectrodes are not used for sensing because droplets are not present over these microelectrodes during bioassay execution.

2) Impact on the Lifetime of MEDA Biochips

We next show that the biochip lifetime can be prolonged using selective sensing. Experimental results on the electrode lifetime in terms of the number of electrode charging are presented in [17]. Based on this study, we consider several scenarios when the microelectrodes in a MEDA biochip can only be charged hundreds of times before they completely break down. From the simulation results, we conclude that if the method described in [19] is used, the most-utilized microelectrode can be charged 196, 262, and 194 times for multiplex in-vitro analysis, ChIP, and gene-expression analysis, respectively. However, when selective sensing is involved, the most-utilized microelectrode was only charged 26, 28, and 21 times for these three bioassays, respectively. We computed the number of bioassay executions for which a MEDA biochip can be used under various worst-case scenarios corresponding to upper limits on the number of times a microelectrode can be charged. The results are shown in Fig. 18. We see that if [19]

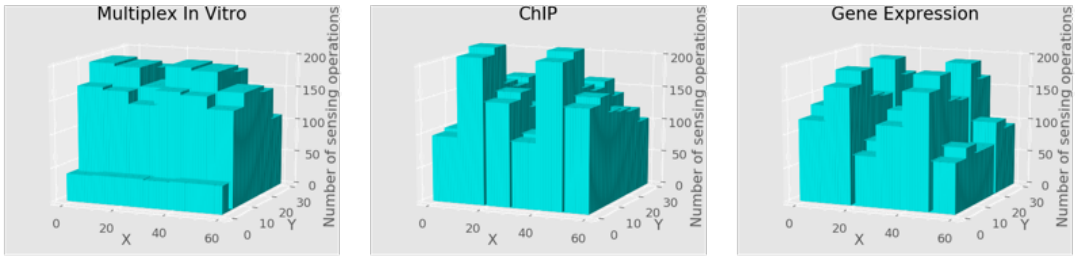

(a)

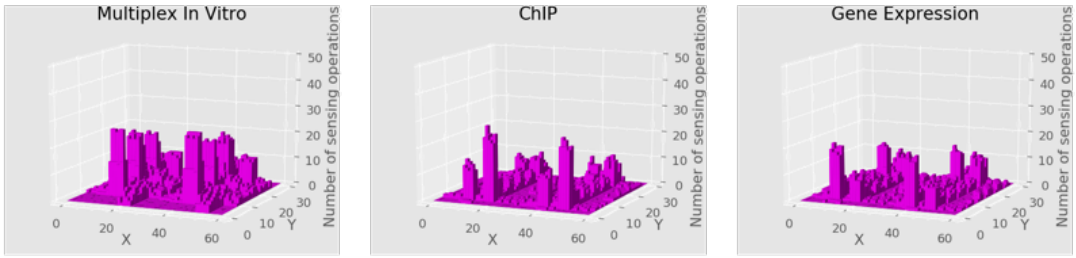

(b)

Fig. 17: The number of sensing operations of each microelectrode after bioassay execution. The x-y plane represents the MEDA biochip, and the z-axis represents the number of sensing operations. (a) Results obtained using the method described in [19]. (b) Results obtained using selective sensing.

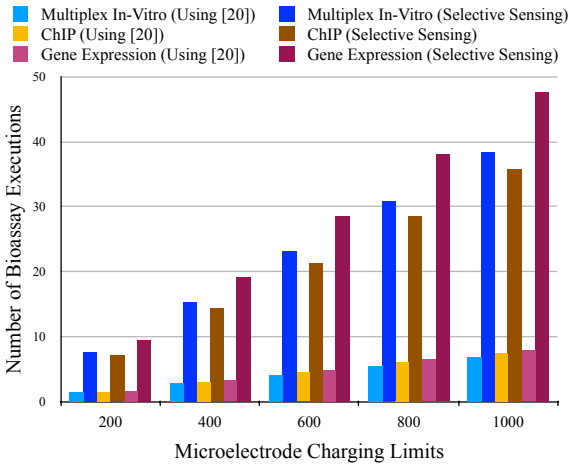

Fig. 18: The lifetime of a MEDA biochip for bioassay execution.

is used, the MEDA biochip can be used for less than nine bioassay executions. In the scenario when the microelectrodes can be charged only 200 times, the MEDA biochip will fail before the bioassay execution is completed. However, when selective sensing is used, we can execute several bioassays on the MEDA biochip before the microelectrodes are degraded. For example, even if the microelectrodes can be charged only 200 times, we can still execute a long bioassay, such as ChIP, seven times on a MEDA biochip. Our results show that selective sensing prolongs the lifetime of a MEDA biochip.

VI. Discussion

In this section, we first examine the overhead associated with selective sensing on a 30×60 MEDA biochip. Next, we discuss the cross-contamination concern in MEDA biochips.

A. Timing Overhead

In the original MEDA biochip, an operational cycle consists of four procedures: 1) the shift of an actuation pattern, 2) microelectrode actuation, 3) sensing operation, and 4) the shift of the sensing result. The scan-chain operates on a 1 MHz clock [9]. Therefore, it takes $1800 \times 10^{-3} = 1.8$ ms to carry out Procedure (1) and Procedure (4). For MEDA biochips, the droplet operations typically take longer time (750 ms) than that needed by CMOS circuits [8]. The sensing operation takes 250 ms [9]. Fig. 19(a) shows the schedule of two consecutive operational cycles. An operational cycle requires a total of 1003.6 ms to finish all the four procedures.

For the proposed selective-sensing method, the operational cycle is longer because we need to scan in an additional sensing pattern before the sensing procedure. The scanning of a sensing pattern also takes 1.8 ms. The new operational cycle is shown in Fig. 19(b). The new overall operational cycle takes 1005.4 ms. The timing overhead of selective sensing is therefore $1.8/1003.6 \times 100\% = 0.18\%$, which is negligible. A biochemical protocol typically consists of hundreds of operational cycles, e.g., 351 cycles for gene-expression analysis. For gene-expression analysis, it takes 352.3 s to execute the bioassay on a conventional MEDA biochip. Using selective sensing, the bioassay now needs an additional 6.3 s. However, the timing overhead is not of a concern even for time-critical immunoassay applications, such as biowarfare detection [36] or point-of-care diagnostics [37], because these bioassays need to be carried out in the time scale of minutes instead of seconds [38].

B. Area Overhead

The original MC contains 36 CMOS transistors and an EDMOS [9]. In the new MC design, the additional gates,

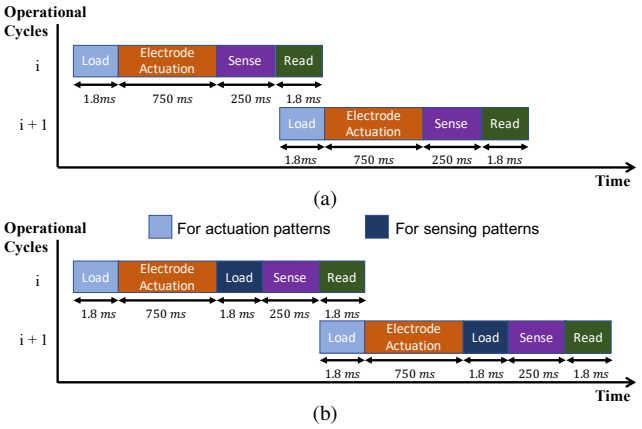

Fig. 19: Timing diagram of two consecutive operational cycles. (a) Original MEDA design. (b) With selective sensing.

a NOT and a 3-input OR, require 10 CMOS transistors. Therefore, the new MC is approximately $46/36 = 1.28$ times larger than the original MC. However, the increased logic footprint is acceptable because it does not affect the fluidic operations on MEDA biochips and neither does it increase the chip footprint. The original MC in [28] was designed in a layout area of $50\times50\,\mu\text{m}$. The proposed new MC requires an area of $(50\times1.28)\times(50\times1.28)\approx64\times64\,\mu\text{m}^2$. According to [39], the radius of the smallest droplet that can be dispensed and moved on MEDA biochips is $70\,\mu\text{m}$. The area of the new MC is therefore still less than the smallest area occupied by a droplet. As a result, all MEDA-enabled operations can be performed on an array composed of the new MCs.

C. Cross-Contamination

Cross-contamination between fluids is a cause of concern for microfluidic biochips. However, this problem can be tackled using a film of inert silicone oil [33]. Electrowetting in oil, instead of in air, is the most-common actuation technique utilized in today's microfluidic biochips [2], [3]. We therefore assume in this paper that cross-contamination does not cause outcome degradation for bioassays. We consider bioassays of longer durations (with hundreds of operational cycles) in this paper. These assays are more likely to be affected by microelectrode degradation. As shown in Section V, electrode degradation may happen before a complex bioassay (e.g., ChIP) is successfully carried out on a MEDA biochip because it requires hundred times of charging in a microelectrode. Therefore, contamination between two bioassays is not of a concern in our work.

VII. Conclusion and Future Work

We have shown that droplet-sensing operations are the predominant contributor to microelectrode degradation in MEDA biochips. Therefore, in order to prolong the lifetime of MEDA biochips, we have presented a selective-sensing method such that only a small fraction of microelectrodes are utilized for droplet sensing during bioassay execution. Simulation results have shown that the total number of droplet-sensing operations is reduced to only 0.7% of the number of such operations required in today's MEDA platform, and the proposed method can prolong the lifespan of a MEDA biochip by as much as 11x.

The proposed selective-sensing method has been implemented based on a new MC design. This design is the first attempt to dynamically enable/disable droplet-sensing operations in MEDA biochips. The new microelectrode cell design and the selective-sensing strategy is likely to result in further optimization based on real-time feedback and probability models. These optimized designs and biochip control strategies will lead to more reductions in the number of droplet-sensing operations and further extend the lifespan of MEDA biochips.

References

[1] W.-L. Chou, P.-Y. Lee, C.-L. Yang, W.-Y. Huang, and Y.-S. Lin, "Recent advances in applications of droplet microfluidics," *Micromachines*, vol. 6, no. 9, pp. 1249–1271, 2015.

[2] R. S. Sista *et al.*, "Digital microfluidic platform to maximize diagnostic tests with low sample volumes from newborns and pediatric patients," *Diagnostics*, vol. 10, no. 1, p. 21, 2020.

[3] S. Huang, J. Connolly, A. Khlystov, and R. B. Fair, "Digital microfluidics for the detection of selected inorganic ions in aerosols," *Sensors*, vol. 20, no. 5, p. 1281, 2020.

[4] C. Quilliet and B. Berge, "Electrowetting: a recent outbreak," *Current Opinion in Colloid & Interface Science*, vol. 6, no. 1, pp. 34–39, 2001.

[5] K. Choi, A. H. Ng, R. Fobel, and A. R. Wheeler, "Digital microfluidics," *Annual Review of Analytical Chemistry*, vol. 5, pp. 413–440, 2012.

[6] "Genmark Official Website," https://www.genmarkdx.com, 2020 [online].

[7] "Baebies Official Website," https://baebies.com, 2020 [online].

[8] G. Wang, D. Teng, and S.-K. Fan, "Digital microfluidic operations on micro-electrode dot array architecture," *IET Nanobiotechnology*, vol. 5, no. 4, pp. 152–160, 2011.

[9] K. Y.-T. Lai, Y.-T. Yang, and C.-Y. Lee, "An intelligent digital microfluidic processor for biomedical detection," *Journal of Signal Processing Systems*, vol. 78, no. 1, pp. 85–93, 2015.

[10] M. Elfar, Z. Zhong, Z. Li, K. Chakrabarty, and M. Pajic, "Synthesis of error-recovery protocols for micro-electrode-dot-array digital microfluidic biochips," *ACM Transactions on Embedded Computing Systems (TECS)*, vol. 16, no. 5s, pp. 1–22, 2017.

[11] Z. Li, K. Y.-T. Lai, J. McCrone, P.-H. Yu, K. Chakrabarty, M. Pajic, T.-Y. Ho, and C.-Y. Lee, "Efficient and adaptive error recovery in a micro-electrode-dot-array digital microfluidic biochip," *IEEE Transactions on Computer-Aided Design of Integrated Circuits and Systems (TCAD)*, vol. 37, no. 3, pp. 601–614, 2017.

[12] Z. Zhong, Z. Li, and K. Chakrabarty, "Adaptive and roll-forward error recovery in MEDA biochips based on droplet-aliquot operations and predictive analysis," *IEEE Transactions on Multi-Scale Computing Systems*, vol. 4, no. 4, pp. 577–592, 2018.

[13] T. Xu and K. Chakrabarty, "Fault modeling and functional test methods for digital microfluidic biochips," *IEEE Transactions on Biomedical Circuits and Systems*, vol. 3, no. 4, pp. 241–253, 2009.

[14] H. Verheijen and M. Prins, "Reversible electrowetting and trapping of charge: model and experiments," *Langmuir*, vol. 15, no. 20, pp. 6616–6620, 1999.

[15] A. I. Drygiannakis, A. G. Papathanasiou, and A. G. Boudouvis, "On the connection between dielectric breakdown strength, trapping of charge, and contact angle saturation in electrowetting," *Langmuir*, vol. 25, no. 1, pp. 147–152, 2009.

[16] F. Su, K. Chakrabarty, and R. B. Fair, "Microfluidics-based biochips: Technology issues, implementation platforms, and design-automation challenges," *IEEE Transactions on Computer-Aided Design of Integrated Circuits and Systems (TCAD)*, vol. 25, no. 2, pp. 211–223, 2006.

[17] C. Dong, T. Chen, J. Gao, Y. Jia, P.-I. Mak, M.-I. Vai, and R. P. Martins, "On the droplet velocity and electrode lifetime of digital microfluidics: voltage actuation techniques and comparison," *Microfluidics and Nanofluidics*, vol. 18, no. 4, pp. 673–683, 2015.

[18] Y.-H. Chen, C.-L. Hsu, L.-C. Tsai, T.-W. Huang, and T.-Y. Ho, "A reliability-oriented placement algorithm for reconfigurable digital microfluidic biochips using 3-D deferred decision making technique," *IEEE Transactions on Computer-Aided Design of Integrated Circuits and Systems (TCAD)*, pp. 1151–1162, 2013.

[19] Z. Zhong, T.-C. Liang, and K. Chakrabarty, "Reliability-oriented ieee std. 1687 network design and block-aware high-level synthesis for MEDA microfluidic biochips," in *Proc. IEEE Asia and South Pacific Design Automation Conference (ASP-DAC)*, 2020.

[20] F. Su and K. Chakrabarty, "High-level synthesis of digital microfluidic biochips," *ACM Journal on Emerging Technologies in Computing Systems (JETC)*, vol. 3, no. 4, pp. 1–32, 2008.

[21] M. Ibrahim, K. Chakrabarty, and K. Scott, "Synthesis of cyberphysical digital-microfluidic biochips for real-time quantitative analysis," *IEEE Transactions on Computer-Aided Design of Integrated Circuits and Systems (TCAD)*, vol. 36, no. 5, pp. 733–746, 2017.

[22] M. Ibrahim, K. Chakrabarty, and U. Schlichtmann, "Synthesis of a cyberphysical hybrid microfluidic platform for single-cell analysis," *IEEE Transactions on Computer-Aided Design of Integrated Circuits and Systems (TCAD)*, vol. 38, no. 7, pp. 1237–1250, 2018.

[23] "Illumina Drop NeoPrep," http://omicsomics.blogspot.com/2017/02/illumina-drops-neoprep.html, 2020 [online].

[24] G. Wang, "Field-programmable microfluidic test platform for point-of-care diagnostics," Ph.D. dissertation, University of Saskatchewan, 2013.

[25] M. G. Pollack, R. B. Fair, and A. D. Shenderov, "Electrowetting-based actuation of liquid droplets for microfluidic applications," *Applied Physics Letters*, vol. 77, no. 11, pp. 1725–1726, 2000.

[26] Z. Li, K. Y.-T. Lai, P.-H. Yu, T.-Y. Ho, K. Chakrabarty, and C.-Y. Lee, "High-level synthesis for micro-electrode-dot-array digital microfluidic biochips," in *Proc. IEEE Design Automation Conference (DAC)*, 2016.

[27] T.-C. Liang, M. Shayan, K. Chakrabarty, and R. Karri, "Secure assay execution on MEDA biochips to thwart attacks using real-time sensing," *ACM Transactions on Design Automation of Electronic Systems (TODAES)*, vol. 25, no. 2, pp. 1–25, 2020.

[28] Z. Zhong, Z. Li, K. Chakrabarty, T.-Y. Ho, and C.-Y. Lee, "Micro-electrode-dot-array digital microfluidic biochips: Technology, design automation, and test techniques," *IEEE Transactions on Biomedical Circuits and Systems*, vol. 13, no. 2, pp. 292–313, 2018.

[29] T.-C. Liang, Y.-S. Chan, T.-Y. Ho, K. Chakrabarty, and C.-Y. Lee, "Multi-target sample preparation using MEDA biochips," *IEEE Transactions on Computer-Aided Design of Integrated Circuits and Systems (TCAD)*, 2019.

[30] J. Gong and C.-J. Kim, "All-electronic droplet generation on-chip with real-time feedback control for ewod digital microfluidics," *Lab on a Chip*, vol. 8, no. 6, pp. 898–906, 2008.

[31] H. Ding *et al.*, "Accurate dispensing of volatile reagents on demand for chemical reactions in EWOD chips," *Lab on a Chip*, vol. 12, no. 18, pp. 3331–3340, 2012.

[32] Z. Li, K. Y.-T. Lai, P.-H. Yu, K. Chakrabarty, T.-Y. Ho, and C.-Y. Lee, "Structural and functional test methods for micro-electrode-dot-array digital microfluidic biochips," *IEEE Transactions on Computer-Aided Design of Integrated Circuits and Systems (TCAD)*, vol. 37, no. 5, pp. 968–981, 2017.

[33] J. Hong, Y. K. Kim, D.-J. Won, J. Kim, and S. J. Lee, "Three-dimensional digital microfluidic manipulation of droplets in oil medium," *Scientific Reports*, vol. 5, p. 10685, 2015.

[34] A. F. Stalder, T. Melchior, M. Müller, D. Sage, T. Blu, and M. Unser, "Low-bond axisymmetric drop shape analysis for surface tension and contact angle measurements of sessile drops," *Colloids and Surfaces A: Physicochemical and Engineering Aspects*, vol. 364, no. 1-3, pp. 72–81, 2010.

[35] "OpenCV Official Website," https://opencv.org/, 2020 [online].

[36] D. N. Stratis-Cullum, G. D. Griffin, J. Mobley, A. A. Vass, and T. Vo-Dinh, "A miniature biochip system for detection of aerosolized bacillus globigii spores," *Analytical Chemistry*, vol. 75, no. 2, pp. 275–280, 2003.

[37] S. K. Sia, V. Linder, B. A. Parviz, A. Siegel, and G. M. Whitesides, "An integrated approach to a portable and low-cost immunoassay for resource-poor settings," *Angewandte Chemie International Edition*, vol. 43, no. 4, pp. 498–502, 2004.

[38] H. C. Feldman, M. Sigurdson, and C. D. Meinhart, "AC electrothermal enhancement of heterogeneous assays in microfluidics," *Lab on a Chip*, vol. 7, no. 11, pp. 1553–1559, 2007.

[39] Z. Zhong, Z. Li, and K. Chakrabarty, "Adaptive error recovery in micro-electrode-dot-array biochips based on droplet-aliquot operations and predictive analysis," in *Proc. IEEE/ACM International Conference on Computer-Aided Design (ICCAD)*, 2017, pp. 615–622.

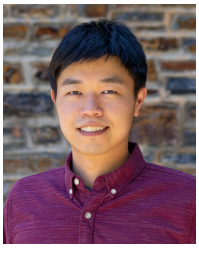

Tung-Che Liang received his B.S. degree in Electronics Engineering from National Chiao Tung University, Hsinchu, Taiwan, in 2014, and the M.S.E. degree from the Department of Electrical and Computer Engineering, Duke University, Durham, NC, USA, in 2020, where he is currently working toward the Ph.D. degree.

He was with Synopsys Inc., Hsinchu, Taiwan, as an R&D engineer. He was a yield & diagnosis intern at Intel, Santa Clara, CA, a DFT intern at NVIDIA Inc., Santa Clara, CA, and a DFT intern at Apple Inc. His current research interests include deep reinforcement learning, design automation, and security for microfluidic systems.

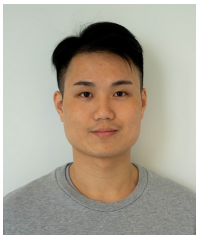

Zhanwei Zhong received the bachelor's degree in electronic science and technology from Sun Yat-sen University, Guangzhou, China in 2013, the master's degree in electronic engineering from Tsinghua University, Beijing, China, in 2016, and the Ph.D. degree in computer engineering from Duke University, Durham, USA, in 2020.

He is currently a senior DFT engineer with Marvell Semiconductor Inc. in Santa Clara, CA, USA. He was a DFT intern with AMD Inc. (Beijing) in 2017 and with Apple Inc. (Cupertino) in 2019. His research interests include design automation for biochips, IJTAG test standard and design verification methodologies.

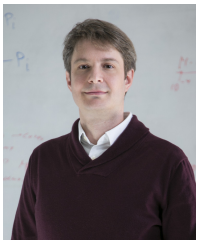

Miroslav Pajic (S'06-M'13-SM'19) received the Dipl. Ing. and M.S. degrees in electrical engineering from the University of Belgrade, Serbia, in 2003 and 2007, respectively, and the M.S. and Ph.D. degrees in electrical engineering from the University of Pennsylvania, Philadelphia, in 2010 and 2012, respectively.

He is currently the Dickinson Family Associate Professor in Department of Electrical and Computer Engineering at Duke University. He also holds a secondary appointment in the Computer Science Department. His research interests focus on the design and analysis of high-assurance cyber-physical systems with varying levels of autonomy and human interaction.

Dr. Pajic received various awards including the ACM SIGBED Early-Career Award, IEEE TCCPS Early-Career Award, NSF CAREER Award, ONR Young Investigator Program Award, ACM SIGBED Frank Anger Memorial Award, Joseph and Rosaline Wolf Best Dissertation Award from Penn Engineering, IBM Faculty Award, as well as seven Best Paper and Runner-up Awards, such as the Best Paper Awards at the 2017 ACM SIGBED International Conference on Embedded Software (EMSOFT) and 2014 ACM/IEEE International Conference on Cyber-Physical Systems (ICCPS), and the Best Student Paper award at the 2012 IEEE Real-Time and Embedded Technology and Applications Symposium (RTAS). He is an associate editor in the ACM Transactions on Computing for Healthcare (ACM HEALTH) and a co-Chair of the 2019 ACM/IEEE International Conference on Cyber-Physical Systems (ICCPS'19).

Krishnendu Chakrabarty (F'08) received the B.Tech. degree from the Indian Institute of Technology Kharagpur, Kharagpur, India, in 1990 and the M.S.E. and Ph.D. degrees from the University of Michigan, Ann Arbor, MI, USA, in 1992 and 1995, respectively.

He is currently the John Cocke Distinguished Professor and the Department Chair of Electrical and Computer Engineering at Duke University, Durham, NC, USA. His current research interests include testing and design-for-test of system-on-a-chip (SOC) integrated circuits, boards, and systems; microfluidic biochips; hardware security; and neuromorphic computing systems.

Prof. Chakrabarty is a Fellow of ACM and AAAS. He is a recipient of the National Science Foundation CAREER Award, the Office of Naval Research Young Investigator Award, the Humboldt Research Award from the Alexander von Humboldt Foundation, Germany, the ACM Transactions on Design Automation of Electronic Systems Best Paper Award in 2017, the IEEE Transactions on CAD Donald O. Pederson Best Paper Award in 2015, over a dozen best paper awards at major conferences, the IEEE Computer Society Technical Achievement Award in 2015, the IEEE Circuits and Systems Society Charles A. Desoer Technical Achievement Award in 2017, and the Semiconductor Research Corporation Technical Excellence Award in 2018. He was an Invitational Fellow of the Japan Society for the Promotion of Science (JSPS) in the Short Term S ("Nobel Prize Level") in 2018.

Prof. Chakrabarty served as the Editor-in-Chief of IEEE Design & Test of Computers during 2010-2012, ACM Journal on Emerging Technologies in Computing Systems during 2010-2015, and IEEE Transactions on VLSI Systems during 2015-2018.